

# Impact of Inversion Domain Boundaries on the Electronic Properties of 3C-SiC

Emilio Scalise,\* Massimo Zimbone, and Anna Marzegalli

**Inversion domain boundaries are extended defects affecting cubic silicon carbide (3C-SiC) layers grown on the on-axis (001) Si wafers. Their impact on the device performance is still debated and a clear connection to their electronic properties at the atomistic scale is still missing. By comparing the first-principles atomistic models and scanning transmission electron microscopy imaging, the most relevant structures of inversion domain boundaries laying both in the {110} and {111} planes are identified. Their calculated electronic structures shed light on the relevance that these extended defects may have in the degradation of the performances of the 3C-SiC devices.**

## 1. Introduction

Extended defects may have a crucial impact on the electronic properties of semiconductors and have been often ascribed as the main cause of poor electronic properties of the cubic silicon carbide (3C-SiC) layers grown on silicon substrates,<sup>[1–3]</sup> possibly causing high leakage current and consequently hindering the use of this SiC polytype for high-power and high-frequency electronics. However, very little is known about the atomic and electronic structure of the various extended defects in 3C-SiC and most of the experimental investigations are not exhaustive in identifying the killer defects for electronics devices and in clarifying their specific impact on the electronic properties of the material. In our previous work<sup>[2]</sup> we exploited a multiscale atomistic approach to investigate one of the main defects affecting the epitaxial 3C-SiC layers, i.e., the stacking

faults (SFs) and in particular focusing on their terminations, so-called dislocation complexes, and revealing that most of them introduce intra-gap states, almost completely filling the electronic bandgap of the 3C-SiC.

Another important class of extended defect that can be found in the epitaxial layer of 3C-SiC is the inversion domain boundaries (IDBs), which have been also suspected to have a very detrimental effect on the electronic properties of 3C-SiC.<sup>[4,5]</sup> In principle, IDBs can be eliminated by orienting the specific polar face of 3C-SiC along a particular direction.<sup>[3]</sup> Still, understanding


their electronic structure is crucial to identify the specific defects degrading the device performance and yield, targeting the efforts to improve the growth process of the 3C-SiC layers. Notice that the lowest energy structure of the IDBs in GaN does not induce electronic states in the bandgap, and would therefore be electrically inert.<sup>[6]</sup> In light of these findings, it is also very interesting to make a comparison with the 3C-SiC case.

We use density functional theory (DFT) to shed light on the electronic properties of the IDBs in 3C-SiC. Different atomistic models are built for IDBs both lying in the {110} and {111} planes and the different configurations have been also compared to high-resolution transmission electron microscopy images. Finally, accurate electronic structure calculations have been performed to overcome the inaccurate bandgap predictions of standard DFT, allowing us to draw important conclusions on the impact of these extended defects on the electronic properties of the 3C-SiC layers.

E. Scalise  
Department of Materials Science  
Università degli Studi di Milano-Bicocca  
via R. Cozzi 55, I-20125 Milano, Italy  
E-mail: emilio.scalise@unimib.it

M. Zimbone  
IMM-CNR  
V. S. Sofia 24, I-95128 Catania, Italy

A. Marzegalli  
L-NESS and Department of Physics  
Politecnico di Milano  
via Anzani 42, I-22100 Como, Italy

 The ORCID identification number(s) for the author(s) of this article can be found under <https://doi.org/10.1002/pssb.202200093>.

© 2022 The Authors. physica status solidi (b) basic solid state physics published by Wiley-VCH GmbH. This is an open access article under the terms of the Creative Commons Attribution-NonCommercial-NoDerivs License, which permits use and distribution in any medium, provided the original work is properly cited, the use is non-commercial and no modifications or adaptations are made.

DOI: 10.1002/pssb.202200093

## 2. Experimental Section

### 2.1. Computational Methods

The electronic structure calculations are based on DFT and exploit the recently developed non-empirical strongly constrained and appropriately normed (SCAN) meta-generalized-gradient approximation (GGA) functionals,<sup>[7]</sup> as implemented in the Quantum Espresso package.<sup>[8]</sup> This allows us to improve the prediction of the bulk SiC bandgap ( $\approx 1.9$  eV) as compared to the value of about 1.35 eV obtained by GGA. The atomistic models were obtained by building supercells of the bulk 3C-SiC and inverting the atomic species of a fractional region, then the ionic position was optimized by using GGA exchange-correlation potentials<sup>[9]</sup> and accounting for the van der Waals interaction by the semiempirical method of Grimme (DFT-D2).<sup>[10]</sup> Within the projector augmented wave (PAW) method,<sup>[11]</sup> plane-wave cutoff energy of 80 Ry was used for the ionic relaxations. The cutoff for the atomic forces

was set to  $10^{-4}$  Ry Bohr $^{-1}$ , exploiting a conjugate gradient method and a  $1 \times 8 \times 1$  or  $8 \times 8 \times 1$  Monkhorst–Pack grid for sampling the Brillouin of the supercells with IDBs lying in the  $\{110\}$  and  $\{111\}$  planes, respectively. The cell optimization had negligible effects both on the formation energy and structure of a few test cases, both for the IDB (110) and IDB (111).

## 2.2. Experimental Methods

3C-SiC was grown heteroepitaxially on silicon using the chemical vapor deposition (CVD) technique, in a horizontal hot-wall reactor in the LPE industry. The (001) Si substrate was a 6 inc 650  $\mu\text{m}$  thick wafer. Hydrogen was used as a carrier gas and the growth process was performed at a pressure and temperature of  $10^4$  Pa and 1370  $^\circ\text{C}$ , after a carbonization step at 1100  $^\circ\text{C}$ . The gases used during the growth were trichlorosilane and ethylene as silicon and carbon precursors. The final 3C-SiC thickness was 30  $\mu\text{m}$ .<sup>[12]</sup> scanning transmission electron microscopy (STEM) was carried out on a JEOL ARM200F probe Cs-corrected transmission electron microscope (TEM), equipped with a cold field emission gun and working at 200 kV. We operated with three detectors, acquiring three images contemporaneously: at low, medium, and high scattering angles. A low angle detector allows us to have bright field (BF) images while the high-angle annular dark field (HAADF) detector (with an inner semi-angle of 80 mrad) was used to obtain the dark-field STEM images. The nominal resolution of the microscope is 0.68  $\text{\AA}$ . In the used configuration, the signal in the image is mainly related to the atomic number  $Z$ , allowing direct identification of the carbon and silicon atomic columns. The images were exported by using the Digital Micrograph Software and analyzed with ImageJ software.<sup>[13,14]</sup>

## 3. Results and Discussions

### 3.1. IDB (110)

Figure 1 illustrates two atomistic models of the IDB lying in the (110) plane. Each periodic supercell contains two IDBs,

highlighted by the dashed lines in Figure 1, where the occupation of Si and C sublattices is reversed. The supercells have 24 and 8 SiC layers along the  $[110]$  directions and  $[001]$  directions, respectively, with 384 atoms. In our models, the minimum distance between the two boundaries is seven layers. The big supercells allowed us to increase this distance up to 12 layers and assess the convergence of the IDB formation energy with the distance, showing an accuracy below  $0.1 \text{ meV } \text{\AA}^{-2}$  for the lower simulated distance, thus even smaller than what had been reported by Lambrecht et al.<sup>[15]</sup>

The upper model in Figure 1 is built by simply inverting the Si and C positions in the region between the two boundaries, but Si–Si and C–C bonds are formed at the interfaces between the two domains. Note that our supercell contains also four periodic replicas along the  $[001]$  direction, thus having a total surface area of the IDB equal to  $53.62 \text{ \AA}^2$ , which is four times the area of the IDB in a unit cell.

In analogy to the GaN case<sup>[6]</sup> we have also modeled the so-called IDB\*, as illustrated in the lower panel of Figure 1, by shifting the atomic planes of one of the two domains by  $a/2$  in the  $[001]$  direction, with  $a$  the lattice constant of 3C-SiC, which is 4.35  $\text{\AA}$  for our lowest-energy bulk structure.<sup>[16]</sup> Although the GaN case is quite different than the 3C-SiC one, both concerning the crystal phase (wurtzite vs. zinc blende) and also the orientation of the IDB, the structural configuration of the IDB and IDB\* is very similar in the two materials: the IDB shows wrong atomic bonds, i.e., between same atomic species, on the boundary surface; while the IDB\* contains fourfold and eightfold rings preventing the wrong bonds of the IDB.

We report in Table 1 the formation energy of the IDB and IDB\*, calculated as  $E_{\text{form}} = (E_{\text{tot}} - E_{\text{bulk}})/2A$ , where  $E_{\text{tot}}$  is the total energy of the structure containing the boundaries (as shown in Figure 1) and  $A$  is the area of its periodic cell in the (110) plane, while  $E_{\text{tot}}$  is the energy of a pristine bulk having the same number of atoms. One may note that the formation energy of the IDB in 3C-SiC is quite similar to the formation energy of the IDB in GaN. The fourfold and eightfold rings of the IDB\* were expected to be much energetically favored as

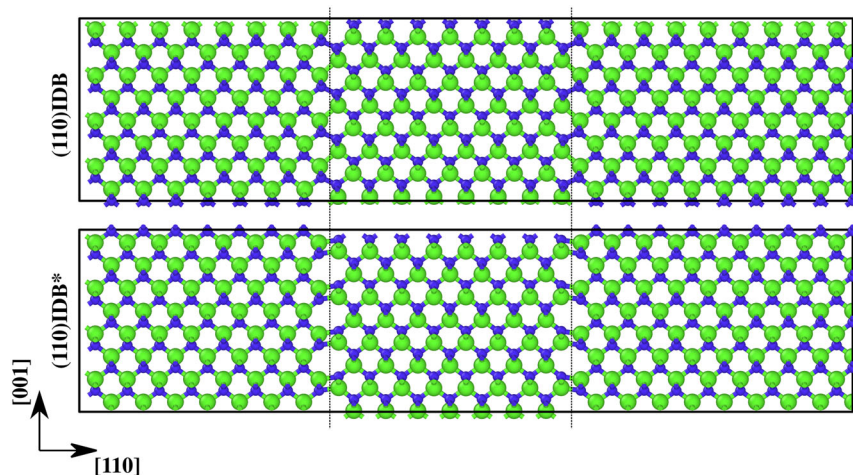


**Figure 1.** Optimized structures of the (110) inversion domain boundaries (IDBs). The IDB\* is the structure obtained via a translation along the  $[001]$  direction, by analogy with ref. [6]. Green and blue spheres represent the Si and C atoms, respectively.

**Table 1.** Formation energies calculated for the IDB and the IDB\* in SiC (our work) and GaN (from ref. [6]).

Material	Type	$E_{\text{form}} [\text{meV } \text{\AA}^{-2}]$
SiC	IDB	140
	IDB*	126
GaN	IDB	167
	IDB*	25

compared to the wrong (Si–Si and C–C) bonds in the IDB. But, we find that the IDB\* has an energy advantage of less than  $15 \text{ meV } \text{\AA}^{-2}$  as compared to the IDB. Still, our experimental analyses revealed several STEM images compatible with the IDB\* atomistic structure, as evident in **Figure 2**, but we have never found anything compatible with the IDB structure.

Even if we can not categorically exclude the presence of the IDB in 3C-SiC epitaxially grown on Si, this indication is even more interesting after looking at the electronic states of the IDB and IDB\* defects. In fact, the calculated band structure shown in **Figure 3** reveals that the IDB\* affects only slightly the band structure of the 3C-SiC, by introducing very shallow defect states, particularly close to the valence band (VB) edge. In fact, the bandgap is only slightly reduced to about 1.6 eV as compared to the bulk case (1.9 eV, as estimated in our calculations<sup>[2]</sup>). Interestingly, very similar conclusions have been drawn for the IDB\* in GaN.<sup>[6]</sup> On the contrary, deep defect states are

evident in the band structure of the IDB, plotted in the top left panel of **Figure 3**, and also in the local density of states (LDOS) integrated into 48 fractional boxes of the supercell along the [110] direction and plotted in the right panels of **Figure 3**. In fact, these defective states are located at real-space positions (15/48 and 30/48 of the supercell size) corresponding to the IDB planes and reduce the bulk bandgap to about 0.75 eV and thus hinting its very bad impact on 3C-SiC-based devices. But, the higher formation energy of the IDB as compared to the (almost) electrical inert IDB\*, which is also confirmed by the lack of the former and the presence of the latter defect in our experimental analysis, suggests that the inversion domain boundaries, particularly lying in the {110} planes may not have a dramatic effect on the electronic properties of 3C-SiC layers grown on Si. Moreover, one may note that the domain wall energy of the IDB\* is estimated at  $126 \text{ meV } \text{\AA}^{-2}$ , a value which is about five times greater than the corresponding energy in GaN. This suggests that the formation of (110) oriented IDB is thermodynamically not very much favored in 3C-SiC. These extended defects may be a consequence of particular growth mechanisms, but not likely “intrinsic” defects in 3C-SiC, contrary to stacking faults, for instance. These latter defects have formation energies of a few tens of  $\text{meV } \text{\AA}^{-2}$ , even becoming negative at high temperatures.<sup>[16]</sup> In contrast, the high formation energy of IDB\* confirm that although these defects may be unavoidable when different nucleation domains merge together during the epitaxial growth on planar Si substrates, they can be completely eliminated if off-cut Si substrates are used.<sup>[3]</sup>

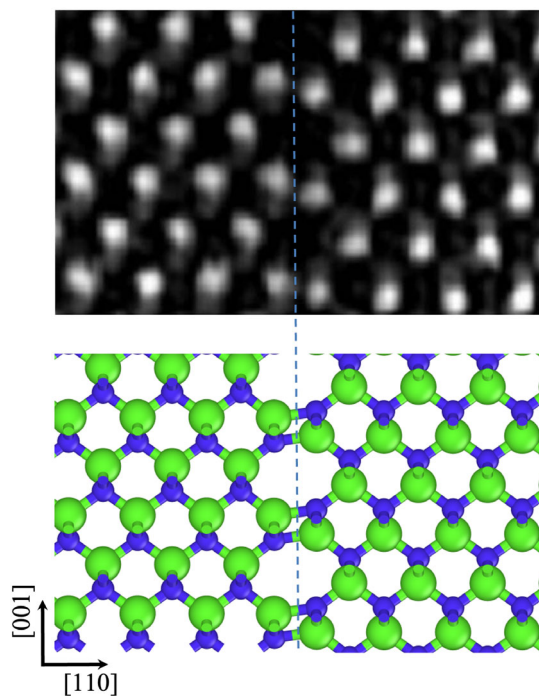


**Figure 2.** High-resolution cross-section high-angle annular dark field-scanning transmission electron microscopy (HAADF-STEM) image of an IDB lying in the (110) plane with its atomic structure model shown below, where green and blue spheres represent the Si and C atoms, respectively.

### 3.2. IDB (111)

Another family of IDBs, which has been recently reported is that one including the extended defects with the domain boundaries lying in the {111} planes.<sup>[14]</sup>

In **Figure 4** the high-resolution STEM images evidence these IDBs and in fact the silicon and carbon sites are inverted in the two regions separated by the dashed horizontal lines in the images of **Figure 4**, representing the IDBs and identifying a (111) plane. The silicon atoms have higher electron scattering cross-sections than carbon atoms, thus they are detectable as larger white halos, while the smaller gray ones are the C atoms.<sup>[13]</sup> The atomistic models corresponding to the STEM images are also shown on the right side of **Figure 4**. It is evident that the IDBs observed in both STEM images are made up of two Si planes forming Si–Si bonds and separating the two regions with inverted domains. Faulted atomic layers are also evident in both STEM images, as also illustrated in their atomistic models. In particular, a single faulted atomic layer, so-called intrinsic stacking fault (ISF),<sup>[16]</sup> is present in the top structure of **Figure 4**. Triple faulted atomic layers, forming the so-called double extrinsic stacking fault (ESFd), are then evident in the bottom STEM image of **Figure 4**. The (111) IDBs look to be peculiarly correlated to the stacking faults (SFs), in fact, all the IDBs lying in {111} planes observed during our investigations are found together with SFs and their number is odd. This aspect could not be confirmed by the total energy calculations of our supercells illustrated in **Figure 5** that model the (111) IDBs without SFs and with the ISF and the ESFd, from left to right side of the figure. In fact,

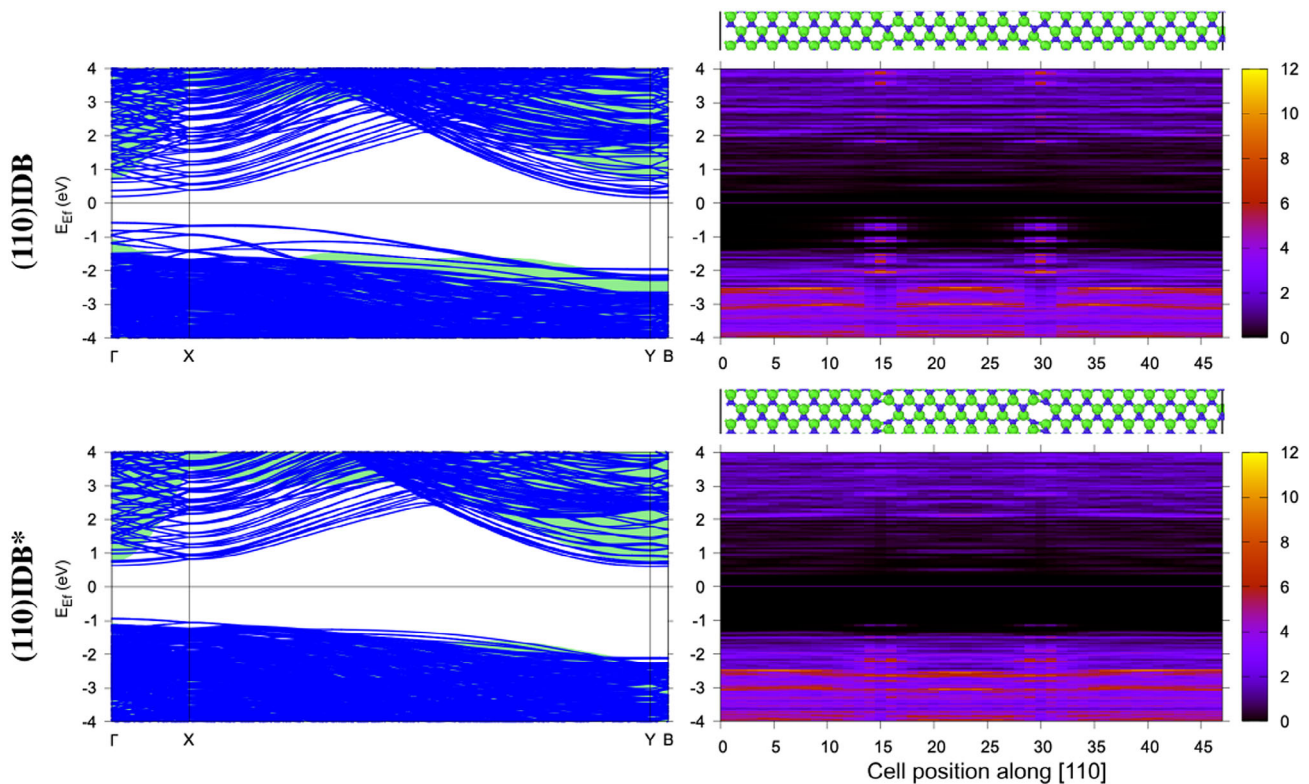


**Figure 3.** The band structures along the high-symmetry lines of the supercells containing the IDB and IDB\* are shown on the left side. The  $\Gamma$ -X line corresponds to the cubic  $[1\bar{1}0]$  direction, the  $\Gamma$ -Y line to the  $[001]$  cubic direction, and the Y-B line corresponds to the  $[110]$  direction of the superlattice. The bulk-projected band structure is also shown for a comparison as a filled curve. On the right side, the integrated LDOS along the  $[110]$  direction of the supercell is shown for the two cases of the IDB and IDB\*, with their planes located at  $15/46$  and  $30/46$  fractional units of the supercell dimension along the  $[110]$  direction. The insets show the atomistic structure aligned with the x-axis of the local density of states (LDOS) plots.

our models have to include both a Si-Si and a C-C boundary in the same cell to form periodic supercells along the  $[111]$  direction. Thus, we cannot calculate the formation energy of a single  $(111)$  IDB and hence compare the formation energy of the different IDBs with Si-Si bonds, but with and without SFs. Moreover, the stability of SFs changes with the temperature<sup>[16]</sup> and their formation and dynamics during the growth process<sup>[2]</sup> may be more important than the ground state energy of the different  $(111)$  IDBs to understand the stability of these latter defects. Thus, more specific theoretical investigations are necessary to elucidate this aspect, but the experimental indications restricting the number of structural cases of  $(111)$  IDBs appearing in the SiC layers are crucial for our electronic analysis of these defects. In **Figure 6**, the band structures and LDOS calculated for the three supercells of Figure 5 shows clearly that several defect states are appearing deeply in the bandgap of the 3C-SiC, reducing its calculated gap up to about 0.36 eV, but most of these states are caused by the C-C bonds. This is the worst case illustrated in the LDOS integrated into boxes, which are fractions of the full supercells along the  $[111]$  direction, and plotted on the right side of Figure 5.

The C-C boundary has been located at about the same  $x$ -axis value 3 for the three simulated supercells, and indeed it is the point where the bandgap has the lowest value (i.e., about 0.41, 0.36, and 0.8 eV for the IDB, IDB + ISF, and IDB + ESF<sub>d</sub>,

respectively). Still, the Si-Si boundaries, which are the only ones observed experimentally, have a less dramatic effect. The bandgap calculated inside the boxes where these boundaries are located (in between 8 and 11  $x$ -values in the plots of Figure 6) varies between 1 eV for the IDB + ISF and 1.5 eV for the IDB + ESF<sub>d</sub>. Note that these ones are the two most interesting cases from the experimental point of view, because the simple  $(111)$  IDB, hence without correlated SFs, has not yet been observed. Thus, our results show that the Si-Si IDB laying in the  $\{111\}$  planes and appearing together with SFs in the experiments have a substantial effect on the band structure of 3C-SiC, introducing defects states and filling about 0.5–1 eV above the valence band edge. Certainly, this has a detrimental impact on the electronic properties of 3C-SiC layers grown on on-axis  $(001)$  Si wafers, but less marked as compared to other extended defects, such as the dislocation complexes,<sup>[2]</sup> thus likely not being the major cause of leakage current in 3C-SiC devices. A different and more destructive impact would be that one of the C-C  $(111)$  IDBs, but they are not probed experimentally.

#### 4. Conclusion

A theoretical study of inversion domain boundaries has been supported by the experimental investigation of 3C-SiC layers

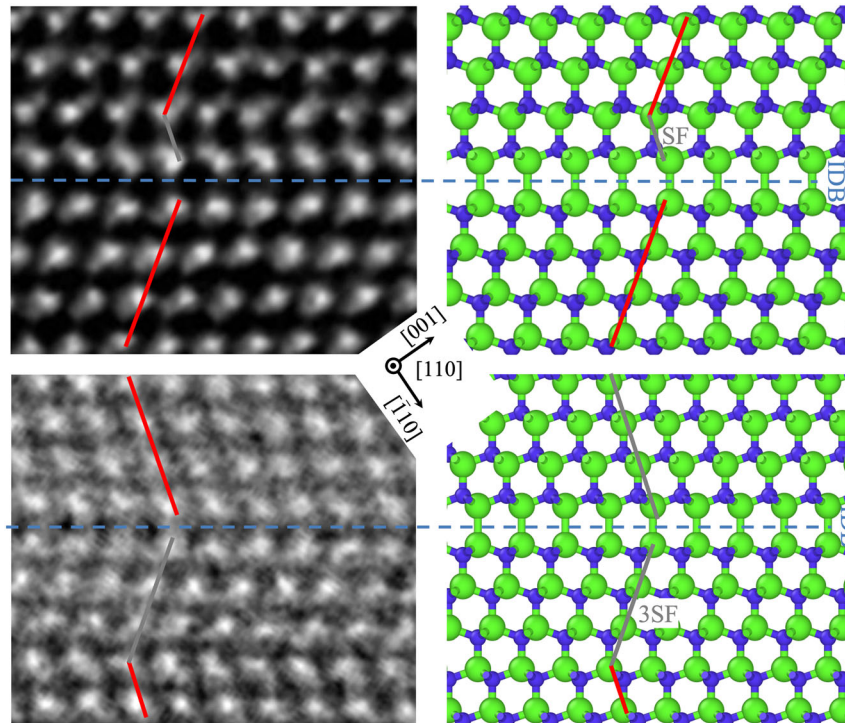


**Figure 4.** High-resolution cross-section HAADF-STEM images of an IDB lying in the (111) plane with the intrinsic stacking fault (ISF) (top) or double extrinsic stacking fault (ESF) (bottom). Their corresponding atomic structure models are shown alongside.

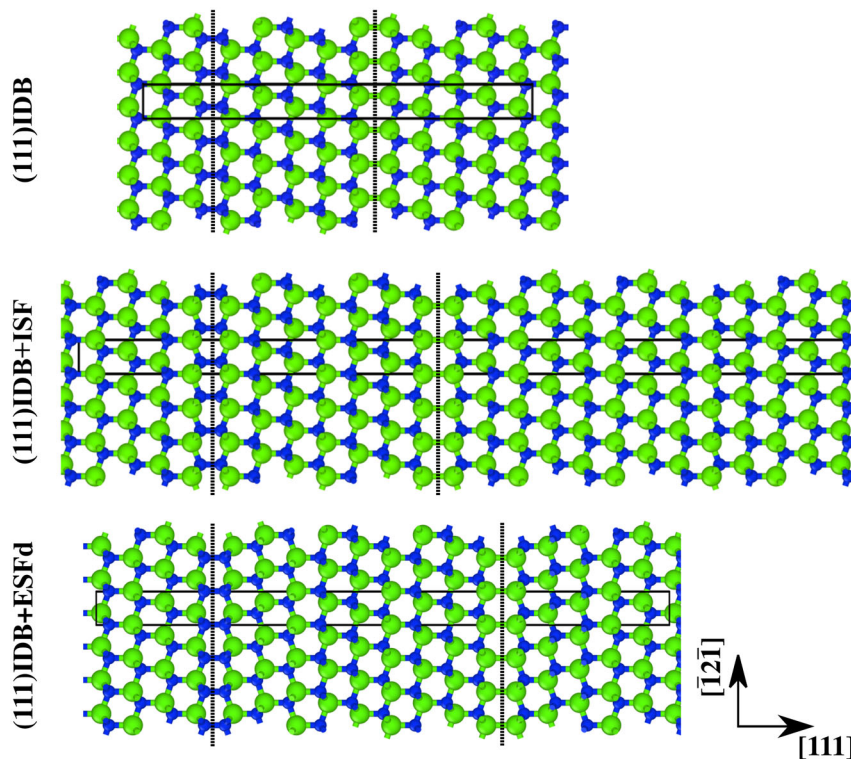


**Figure 5.** Optimized structures of the (111) IDBs. Green and blue spheres represent the Si and C atoms, respectively. The simulated supercell units are also shown by solid lines, while dashed lines indicate the IDB planes.

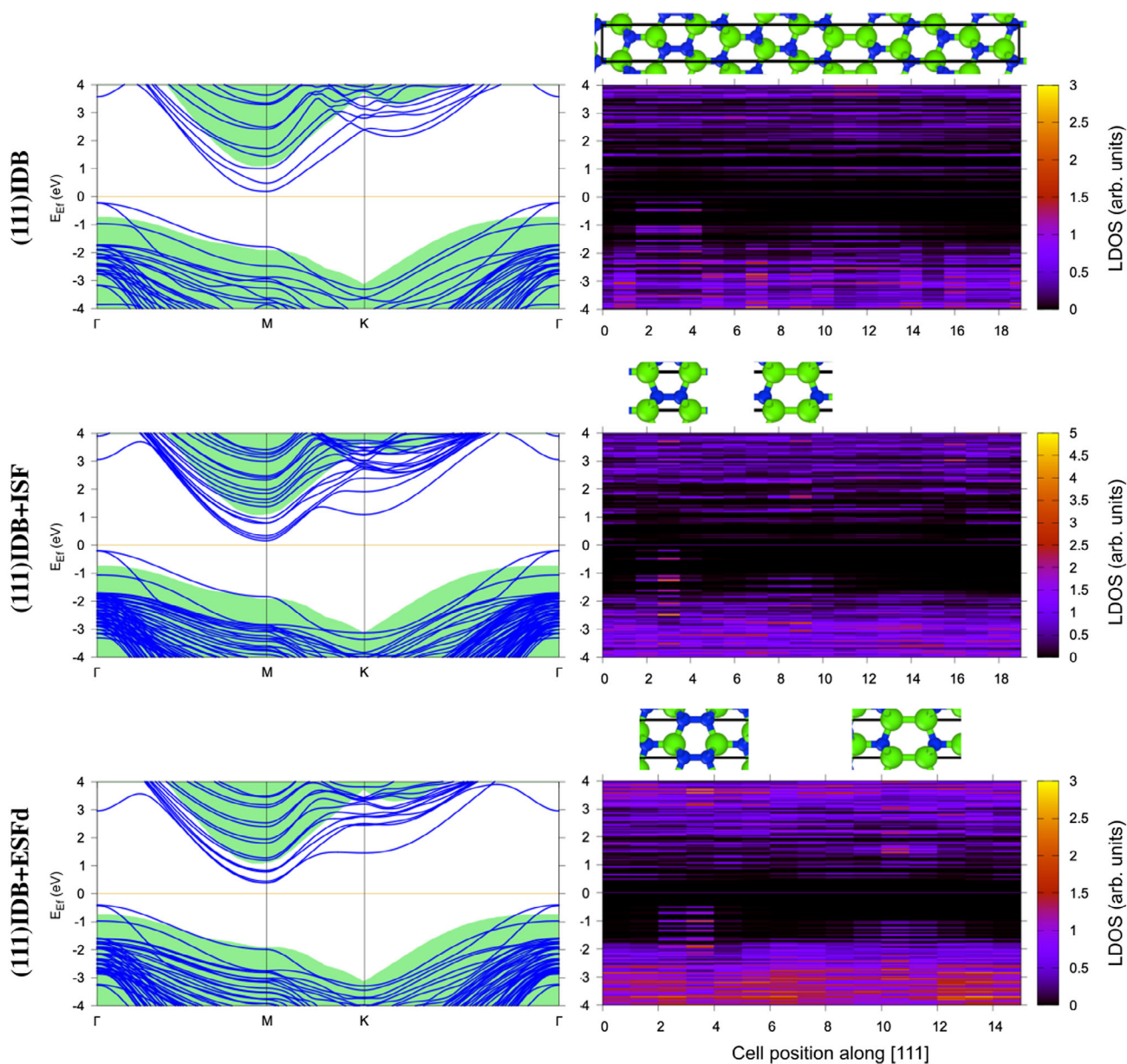


**Figure 6.** The band structures along the high-symmetry lines of the supercells containing the (111) IDBs. The  $\Gamma$ -M line corresponds to the cubic [111] direction, the  $\Gamma$ -K line to the cubic [001] direction. The bulk-projected band structure is also shown for comparison as a filled curve. On the right side, the integrated LDOS along the [111] direction of the supercell is shown for the three cases of the IDB, IDB with ISF, and ESFd. The IDB planes containing the C-C bonds are located at  $3/20$  (or  $3/16$  for the IDB + ESFd) fractional units of the supercell dimension along the [111] direction. The IDB planes containing the Si-Si bonds are located at about  $12/20$ ,  $9/20$ , and  $9/16$  fractional units of the supercell dimension along the [111] direction, for the IDB, IDB + ISF and IDB + ESFd, respectively. The insets show the atomistic structure aligned with the x-axis of the LDOS plots, focusing on the IDBs.

grown on the on-axis (001) Si wafers. Different atomistic models of the IDBs are compared to the high-resolution cross-section HAADF-STEM images, allowing us to identify a subset of them that are undoubtedly present in the 3C-SiC layers for both families of IDBs laying in the {110} and {111} crystallographic planes. For the (110) IDBs, a structure named IDB\* has been found to be slightly more stable than the simpler model and it is also the only one so far observed experimentally. The IDB\*, similarly to the GaN case, only slightly affect the band structure of the 3C-

SiC, and hence it is improbable that they have a detrimental effect on the electronic properties of the devices. For the IDBs lying in the {111} planes, the calculations are not effective in building a hierarchy of the thermodynamic stability of the possible structures of these defects, but experimentally it is quite evident that these boundaries have always a Si-Si bonding front and they are correlated to SFs, particularly ISF and ESFd. The electronic properties simulated for these (111) IDBs show more pronounced signatures as compared to the (110) IDB\*, forming a

defects band up to 1 eV above the valence band of the 3C-SiC. Although this may have important effects on the functioning of devices, IDBs are not likely the main cause of high-leakage current and failure of 3C-SiC devices. In fact, it has been shown that dislocation complexes terminating the SFs have an even higher impact on the electronic properties of 3C-SiC and contrary to the IDBs, they cannot be eliminated by using off-axis (001) Si substrates.<sup>[17–19]</sup>

## Acknowledgements

The authors acknowledge the CINECA award under the ISCRA initiative, for the availability of high-performance computing resources and support. This work has been partially supported by the CHALLENGE project (HORIZON 2020-NMBP-720827, <http://www.h2020challenge.eu/>), CHALLENGE is a research and innovation action funded by the European Union Horizon 2020 program. The authors gratefully acknowledge the scientific support of Dr. F. La Via and Prof. L. Miglio.

Open Access Funding provided by Università degli Studi di Milano-Bicocca within the CRUI-CARE Agreement.

## Conflict of Interest

The authors declare no conflict of interest.

## Data Availability Statement

The data that support the findings of this study are available from the corresponding author upon reasonable request.

## Keywords

density functional theory, extended defects, inversion domain boundaries, SiC, wide-bandgap

Received: March 2, 2022

Revised: May 11, 2022

Published online:

[1] W. R. L. Lambrecht, B. Segall, *Phys. Rev. B* **1990**, 41, 2948.

- [2] E. Scalise, L. Barbisan, A. Sarikov, F. Montalenti, L. Miglio, A. Marzegalli, *J. Mater. Chem. C* **2020**, 8, 8380.
- [3] H. Nagasawa, R. Gurunathan, M. Suemitsu, *Mater. Sci. Forum* **2015**, 821–823, 108.
- [4] F. Giannazzo, G. Greco, S. Di Franco, P. Fiorenza, I. Deretzis, A. La Magna, C. Bongiorno, M. Zimbone, F. La Via, M. Zielinski, F. Roccaforte, *Adv. Electron. Mater.* **2020**, 6, 1901171.
- [5] F. La Via, M. Zimbone, C. Bongiorno, A. La Magna, G. Fiscaro, I. Deretzis, V. Scuderi, C. Calabretta, F. Giannazzo, M. Zielinski, R. Anzalone, M. Mauceri, D. Crippa, E. Scalise, A. Marzegalli, A. Sarikov, L. Miglio, V. Jokubavicius, M. Syväjärvi, R. Yakimova, P. Schuh, M. Schöler, M. Kollmuss, P. Wellmann, *Materials* **2021**, 14, 5348.
- [6] J. E. Northrup, J. Neugebauer, L. T. Romano, *Phys. Rev. Lett.* **1996**, 77, 103.
- [7] Y. Yao, Y. Kanai, *J. Chem. Phys.* **2017**, 146, 224105.
- [8] P. Giannozzi, S. Baroni, N. Bonini, M. Calandra, R. Car, C. Cavazzoni, D. Ceresoli, G. L. Chiarotti, M. Cococcioni, I. Dabo, A. Dal Corso, S. De Gironcoli, S. Fabris, G. Fratesi, R. Gebauer, U. Gerstmann, C. Gougoussis, A. Kokalj, M. Lazzeri, L. Martin-Samos, N. Marzari, F. Mauri, R. Mazzarello, S. Paolini, A. Pasquarello, L. Paulatto, C. Sbraccia, S. Scandolo, G. Sclauzero, A. P. Seitsonen, et al., *J. Phys.: Condens. Matter* **2009**, 21, 395502.
- [9] J. P. Perdew, K. Burke, M. Ernzerhof, *Phys. Rev. Lett.* **1996**, 77, 3865.
- [10] S. Grimme, *J. Comput. Chem.* **2006**, 27, 1787.
- [11] P. E. Blöchl, *Phys. Rev. B* **1994**, 50, 17953.
- [12] M. Zimbone, M. Mauceri, G. Litrico, E. G. Barbagiovanni, C. Bongiorno, F. La Via, *J. Cryst. Growth* **2018**, 498, 248.
- [13] M. Zimbone, E. G. Barbagiovanni, C. Bongiorno, C. Calabretta, L. Calcagno, G. Fiscaro, A. La Magna, F. La Via, *Cryst. Growth Des.* **2020**, 20, 3104.
- [14] M. Zimbone, A. Sarikov, C. Bongiorno, A. Marzegalli, V. Scuderi, C. Calabretta, L. Miglio, F. La Via, *Acta Mater.* **2021**, 213, 116915.
- [15] W. R. Lambrecht, B. Segall, *Phys. Rev. B* **1990**, 42, 1462.
- [16] E. Scalise, A. Marzegalli, F. Montalenti, L. Miglio, *Phys. Rev. Appl.* **2019**, 12, 021002.
- [17] H. Nagasawa, M. Abe, K. Yagi, T. Kawahara, N. Hatta, *Phys. Status Solidi B* **2008**, 245, 1272.
- [18] K. Shibahara, S. Nishino, H. Matsunami, *J. Cryst. Growth* **1986**, 78, 538.
- [19] J. A. Powell, L. G. Matus, M. A. Kuczmarski, C. M. Chory, T. T. Cheng, P. Pirouz, *Appl. Phys. Lett.* **1987**, 51, 823.